A multi-wavelength streak-optical-pyrometer for warm-dense matter experiments at NDCX-I and NDCX-II

P.A. Ni, F.M. Bieniosek, E. Henestroza and S. M. Lidia
Lawrence Berkeley National Laboratory, Berkeley, CA, USA

Abstract
We report on a multi-wavelength streak-optical-pyrometer (SOP) developed the for warm-dense-matter (WDM) experiments at the existing NDCX-I facility and the NDCX-II facility currently being commissioned at LBNL. The SOP served as the primary temperature diagnostic in the recent NDCX-I experiments, in which an intense K^+ beam was used to heat different metal samples into WDM states. The SOP consists of a spectral grating (visible and near-infrared spectral range) and a fast, high-dynamic-range optical streak camera. The instrument is calibrated absolutely with a NIST-traceable tungsten ribbon lamp and can itself be considered as an absolutely calibrated, time-resolving spectrometer. The sample temperature is determined from fitting the recorded thermal spectrum into the Planck formula multiplied by a model of emissivity.

Introduction
Warm dense matter (WDM) is characterized by near solid-state density, temperature up to 100,000 K and several Mbar pressure. These states are relevant to the fields of plasma physics, astrophysics, geophysics, planetary science, etc. [Davidson]. An extensive WDM research campaign with intense heavy ion beams was launched at the Lawrence Berkeley National Laboratory (LBNL) in 2008 [Bieniosek]. The ultimate goal of these experiments is to investigate properties of matter under extreme conditions. In particular, the near term goal is to study the equation of state (EOS) of various metals near melting, in the two-phase liquid-vapor and critical regions of the phase diagram. In general, temperature, pressure and density must be known for a complete thermodynamic description of matter. This paper focuses on temperature diagnostic and in particular, on a recently fielded multi-wavelength streak optical pyrometer (SOP).

The Neutralized-Drift-Compression-eXperiment-I accelerator (NDCX-I) (Figure 1), generates 300 keV, 30 mA beams of K^+ ions [Seidl], which when focused to a 1 mm spot, can heat metal targets up to 0.5 eV. During the course of an experiment, a sample passes through melting, evaporation and solidification phases. Depending on the objective of an experiment, ion beam bunch duration can be varied from 2 ns to tens of microseconds (Figure 2). The 300 keV beam energy allows for uniform, volumetric heating of samples as thick as 100 nm.

The Neutralized Drift Compression eXperiment-II (NDCX-II), is a next-generation linear induction Li^+ accelerator at LBNL [Friedman, Waldron]. NDCX-II will have sufficient beam energy to heat a few-micrometer-thick sample to temperatures up to 10 eV. True isochoric heating will be possible at NDCX-II, since the ion beam pulse length can be as short as 300 ps, which is less than the hydro-response time of a micrometer-thick sample. When the commissioning phase is complete in 2013, NDCX-II will be run as a U.S. Department of Energy (DOE) national user facility for High Energy Density physics

(HEDP), inertial confinement fusion (IFE), and intense beam physics research. The developed SOP will be a primary temperature diagnostic in the WDM experiments at this future facility.

Experimental setup

A layout of the experiment is shown in Figure 3. A sample is heated by a focused ion beam in a vacuum chamber; a relay glass-lens system collects the thermal emission from the sample and focuses it on a multi-mode optical fiber. Depth of field of the collection optics is ~ 1 mm, while thickness of a target in various experiments ranged from 50 nm to 5 μm. The fiber transports the light outside the chamber and connects to a spectral grating (Horiba Jobin Yvon, CP-140); the resolved spectrum is projected on a slit of an optical streak camera (Hamamatsu C7700), which records the temporal evolution of the emission spectrum. The holographic grating is etched directly onto an off-axis parabola – this arrangement is convenient and efficient, as it allows for spectral resolution and focusing by the same optical element. In addition, the dispersion law of the grating is linear, making the data processing easier and spectral resolution independent of a wavelength. The grating is mounted on a x-y-z linear micrometer-stage, allowing for a selection of a specific spectral range (x-direction movement), a focal adjustment (z-direction movement) and a height adjustment to the slit (y-direction movement), see Figure 3.

The length of the entrance slit of the camera (x-direction), as well as width of the slit (y-direction) can be adjusted with micrometers. The length of the slit primarily determines the spectral span, which is ~400 nm, when the slit length is at its maximum opening (14.5 mm). The covered region can be adjusted ±100 nm by moving the grating along the slit. The low band sensitivity cut-off of the streak cathode (as well as that of the grating) is ~200 nm; the high band cut-off is 950 nm. In the recent NDCX-I experiments the grating was tuned for the 430 nm-850 nm range. A 435-nm-long-pass filter, placed in front of the slit, blocks the higher reflection orders of the grating. The present setup is tuned for the "low" temperature (<0.5 eV) NDCX-I experiments. In this temperature range most of thermal emission is concentrated in the visible and near-infrared parts of the spectrum, thus justifying the 430 nm-850 nm range. In the future NDCX-II experiments, the target temperature can be as high as 10 eV, requiring the spectral band to be in the UV region. In this case, the internal camera optics will have to be replaced with those optimized for the UV range (available as an option from the manufacturer).

Spectral resolution of the instrument is determined primarily by the diameter of a fiber. During the course of experiments at NDCX-I, the fiber size ranged from Ø50 μm to Ø600 μm, with corresponding resolution changing from 1 nm to 20 nm. This resolution is sufficient for the recording of a continuous thermal spectrum, meanwhile for a finer, sub-nm resolution (e.g. necessary for measurements of line shift and line broadening), a fiber with smaller diameter should be used. Temporal resolution of the SOP is determined by a streak sweep time, slit width and the pixel resolution of the CCD chip. Slit width used in the experiment was ~10 pixels, which is a reasonable balance between level of a signal and temporal response. Depending on the experimental conditions, the sweep time was varied between 1 μs and 20 μs, which corresponds to 10 ns and 200 ns temporal

resolution respectively (these times are consistent with several nanoseconds modal dispersion occurring in a typical 5 m-long, multi-mode fiber). The ~2% of non-linearity in the temporal sweep (i.e. relation between time and vertical pixels of a camera) is corrected *in situ* by the camera software, which uses calibration files provided by the manufacturer.

The cooled CCD camera has a 14 bit gradation, providing a remarkably high dynamic range: maximum pixel count is 16,384 while a typical noise level (depends on the gain setting) is ~100 counts. This high dynamic range allows for a measurement of a broad, ~5000 K temperature span. Depending on the wavelength, the lowest detectable black body temperature can be as low as ~1200 K. The streak camera has a large two-stage internal gain (one micro-channel-plate (MCP) is in the streak unit and one MCP is in the camera) and can be operated in a single-photon-counting mode. For a comparison, the overall sensitivity of the system can be close or exceed that of a photo multipliers tube.

Calibration

Two types of instrument calibration are necessary: the spectral calibration, which relates horizontal pixels to a wavelength, and an absolute calibration, which connects CCD counts with absolute radiation power.

The spectral calibration establishes connection between horizontal pixel coordinates, x (from 1 to 1344) and wavelength, λ in nanometers. The calibration is performed with an Ar-Hg lamp (Ocean Optics CAL-2000), a CW source that emits in the known spectral lines (Figure 4). While the dispersion law of the grating is linear, chromatic and spherical aberrations of the internal relay lens systems of the camera introduce a certain degree of non-linearity into the pixel-wavelength relation. It was found that a cubic polynomial describes this relation reliably. The final function $\lambda(x)$ is determined from fitting the streak lines (at least 10 lines) to the corresponding lines of the lamp spectrum.

The absolute calibration relates pixel counts to actual spectral energy density (in units of W/cm^2/nm/sr) irradiated by the sample in a real experiment. The absolute calibration of the SOP is carried out with a tungsten ribbon lamp at 2600 K [Ni, Dewitt]. The lamp is a NIST-traceable calibration standard and its absolute spectral density, $L_{NIST}(\lambda)$ is known with 1%-3% precision (Figure 5a). Once the lamp is in thermal equilibrium, a set of raw streak images, C^{calibr}, are taken for various gains and fiber sizes (Figure 5b). The resulting calibration file, S is a 1024x1344 matrix (Figure 5c), in which each x-y element is in " W/cm^2/nm sr/pixel-count" units, and calculated as

$$S(x,y) = L_{NIST}(\lambda(x)) / C^{calibr}(x,y) .$$

The calibration file S also includes the inherent flat-field correction (shadowing caused by imperfections of the internal optics, such as geometric aberrations, chromatic aberrations, etc) as well as corrections reflecting sensitivity changes of the camera acquired during its life time (photocathode dirt, damage and degradation). All optical components, including, collections optics, grating, fiber, vacuum feed-throughs, etc.,

were used during the calibration procedures, and their transmission is already included in the calibration image.

The streak camera has a low degree of non-linearity response (as low as 2%), making the data processing straightforward. The absolute spectrum, *I* recorded in a real experiment is derived from the raw-count image, *C* as

$$I(x,y) = C(x,y) \cdot S(x,y) .$$

Experimental results

Experiments with various pulse shapes, materials (Pt, Au, W, C, Nb, Si), sample thicknesses (50nm, 100 nm,150nm, 500 nm, 1 μm 3 μm) were performed using the NDCX-I beam as a driver. Figure 6 shows SOP records in two experiments with a 100 nm-thick gold target (the ion beam is stopped completely in the foil). In these experiments the beam was focused to a Ø1 mm spot and two different heating modes (beam temporal pulse profiles) were used. In the first experiment (Figure 6, left), the uncompressed part of the ion pulse was bunched to a 2 ns pulse similarly to the pulse shape shown in Figure 2. A sharp thermal emission peak is seen at 3 μs – a moment when the compressed pulse arrived; the peak is preceded by weaker emission coming from pre-heat by an uncompressed pulse. Figure 6 (right) shows the thermal emission recorded in an experiment, in which no bunching was used and heating was done by the uncompressed part of the beam only.

Records in Figure 6 contain the emission in absolute units, allowing for an immediate calculation of the black body temperature [Dewitt]. In reality, the emission differs from the idealized black body model, which provides only a rough estimate of the true temperature – a more precise temperature estimate requires knowledge of spectral emissivity [Michalski]. A common approach to temperature measurements, in which emissivity ε is not known, is to approximate it by a polynomial function (here, polynomial coefficients and the temperature are fitting variables). Following this recipe, temperature is determined for each instance of the record in Figure 6 by curve-fitting the spectrum into a Planck formula multiplied by a emissivity, represented by a power two polynomial [Ni].

$$I\ (x, y = t) \xrightarrow{\text{least-square fit}} \varepsilon(\lambda) \cdot \frac{C_1}{\lambda^5} \frac{1}{e^{\frac{C_2}{\lambda T}} - 1},$$

$$\varepsilon(\lambda) = A_2 \cdot \lambda^2 + A_1 \cdot \lambda + A_0 .$$

Data processing: for each instance, *t*, the recorded spectra, *I* is a least-square fit into the emission model, in which emissivity is a power two polynomial. A_i and T – fit parameters; C_i –are the Plank formula constants.

Figure 7 shows the measured spectrum for various instances of time and the corresponding best-fitted curve into the emission model with a quadratic dependence of emissivity on λ. Figure 8 shows the temperature resulting from the curve-fitting of the spectrum in Figure 6 (left). The error-bar associated with fitting procedure ranges from

3% to 10% (highest value is at the end of record when the signal becomes lower). For a comparison, black body temperature for various wavelength, numerical simulations, as well as beam current, are also shown.

Discussion

According to temperature values in the Figure 8, the gold target was melted (T_{melt}=1337 K) and eventually heated close to the boiling point (T_{boil}=3129 K). Due to the large surface-to-thickness aspect ratio of a sample (target thickness is 100 nm; beam spot is Ø1 mm) the surface tension of the melted gold tears the foil apart and eventually breaks it into droplets [Bieniosek2]. A separate laser transmission experiment determined that the disassembly of the foil occurs approximately after 600 ns relative to the head of the beam. The NDCX-I ion beam, which lasts for several microseconds, continues heating the droplets accompanied by an intense surface evaporation of Au. At the later stages of the experiment, the target is a cloud of droplets of various sizes emerged in gold vapor.

The discrete atomic lines in Figure 6 were identified as the atomic neutral gold lines. The presence of these lines can be explained by the gold vapor: the neutral gold atoms are excited by the collision with the K^+ ion passing though the vapor mix. This beam-induced excitation has been confirmed in a different experiment, in which beam current was temporally modulated and the registered temporal behavior of the line emission was consistent with the beam current modulation. In the fitting procedures, those parts of spectrum corresponding to lines were excluded from the data processing. The delayed time appearance of the lines can be explained by the finite time for the voids in the foil to develop to a degree, at which sufficient number of ions can pass through the target and excite the vapor atoms.

The lower value of the fitted temperature from the simulated temperature can be explained by the droplet formation. While theory assumes an undamaged flat foil and constant energy deposition rate, in practice, the void between droplets reduces the effective ion absorption area, resulting in the reduced energy deposition rate. Also the energy lost through evaporation is higher, since the total evaporation area of a droplet cloud is large than that of a flat unbroken foil.

In Figure 8, there is a noticeable difference between the temporal behavior of the black body temperature and the fitted temperature after the 3μs mark: the brightness temperature drops abruptly after the pulse, while the fitted one decays slower, in the expected "thermal" fashion. From a physical standpoint, there is no obvious reason for such a rapid "cool down", which is yet seen in the brightness temperature records. This sudden drop can be explained by a geometrical factor. Energy delivered by the compressed pulse results in a higher heating rate and consequently in a higher evaporation rate, which leads to droplet size reduction and accelerated expansion of the droplet cloud. As the result, the number of emission centers (i.e. droplets) within the optics probing spot (Ø200 μm) decreases (vapor is transparent and does not emit light), leading to the decrease in the registered emission intensity. Remarkably, this decrease is not related to the change in temperature but caused solely by the geometrical phenomena. Here an advantage of the spectral fitting is obvious: in contrast to black-body

temperature, which is based solely on the absolute values at a fixed wavelength, the multi-wavelength curve-fitting exploits primarily the (relative) shape of the spectrum, which contains the true temperature information, thus allowing to exclude the geometrical effects. Emissivity, obtained in the fitting procedure, already contains the geometrical correction. For this reason, emissivity is not shown and not discussed in this paper, because the obtained absolute value of emissivity does not reflect the optical properties of the target.

Summary

The developed SOP has been successfully commissioned in the recent NDCX-I experiments. It will be a main temperature diagnostic in the upcoming WDM experiments at the NDCX-II.

Acknowledgments.

Authors sadly note the untimely passing of our friend, colleague, and co-author Frank Bieniosek. His clarity of scientific vision, his energy and enthusiasm, his guidance, and his companionship are much missed. Author would like to thank Tak Takayanagi and Ahmet Pekedis for assisting with the experimental setup and Mikhail Kulish and Dimitry Nikolaev of Institute of Problems of Chemical Physics, Russia, for the technical discussions. This work was performed under auspices of the U.S. Department of Energy under Contract No. DE-AC02-05CH11231.

References

[Davidson] Frontiers in High Energy Density Physics: The X-Games of Contemporary Science, Committee on High Energy Density Plasma Physics, Plasma Science Committee Board on Physics and Astronomy, Division on Engineering and Physical Sciences (2003) NATIONAL RESEARCH COUNCIL OF THE NATIONAL ACADEMIES

[Bieniosek1] F. M. Bieniosek, J. J. Barnard, J. E. Coleman, E. Henestroza, M. A. Leitner, B. G. Logan, R. M. More, P. A. Ni, P. K. Roy, W. L. Waldron, P. A. Seidl, "High Energy Density Physics Experiments with Intense Heavy Ion Beams", Heavy Ion Fusion Symposium 2008, Tokyo,Japan, August 2–9, 2008.

[Seidl] P. A. Seidl, A. Anders, F. M. Bieniosek, J. J. Barnard, J. Calanog, A. X. Chen, R. H. Cohen,J. E. Coleman, M. Dorf, E. P. Gilson, D. P. Grote, J. Y. Jung, M. Leitner, S. M. Lidia, B. G.Logan, P. Ni, P. K. Roy, K. Van den Bogert, A. B. Sefkow, W. L. Waldron, D. R. Welch,"Progress In Beam Focusing and Compression for Warm-Dense Matter Experiments", Heavy Ion Fusion Symposium 2008, Tokyo, Japan, August 2–9, 2008.

[Friedman] A. Friedman, J. J. Barnard, R. H. Cohen, D. P. Grote, S. M. Lund, W. M. Sharp, A. Faltens, E. Henestroza, J.-Y. Jung, J. W. Kwan, E. P. Lee, M. A. Leitner, B. G. Logan, J.-L. Vay, W. L. Waldron, R. C. Davidson, M. Dorf, E. P. Gilson, and I. D. Kaganovich, Phys. Plasmas 17, (2010).

[Ni] P.A. Ni, M.I. Kulish, V. Mintsev, D.N. Nikolaev, V.Ya. Ternovoi, D.H.H. Hoffmann, S. Udrea, A. Hug, N.A. Tahir and D.H.H. Hoffmann, Temperature measurements of warm-dense-matter generated by heavy-ion beams, Laser and Particle Beams 26 (04), 583 - 589 (2008).

[Dewitt] D. P. Dewitt, "Theory and practice of radiation thermometry", John Wiley & Sons, Inc., (1998).

[Michalski]L. Michalski, K. Eckersdorf, J. Kucharski, J.McGhee, Temperature Measurement, Second Edition, 2001 John Wiley

[Bieniosek2] F.M. Bieniosek, J.J. Barnard, A. Friedman, E. Henestroza, J.-Y. Jung, M.A. Leitner, S. Lidia, B.G. Logan, R.M. More, P.A. Ni, P.K. Roy, P.A. Seidl, W.L. Waldron, “Ion-beam-driven warm dense matter experiments”, IFSA 2009, 2010 J. Phys.: Conf. Ser. 244 032028. HIFAN 1747, LBNL-2378E.

[Waldron] W.L. Waldron, W.J. Abraham, D. Arbelaez, W.G. Greenway, J.-Y. Jung, J.W. Kwan, M.L. Leitner, S.M. Lidia, T.M. Lipton, L.R. Reginato, M.J. Regis, P.K. Roy, M.W. Stettler, J.H. Takakuwa, J. Volmering, V.K. Vytla, “The NDCX-II Engineering Design”, Proceedings of the 2012 Heavy Ion Fusion Symposium, Berkeley, submitted to *Nuclear Instruments and Methods in Physics Research A*.

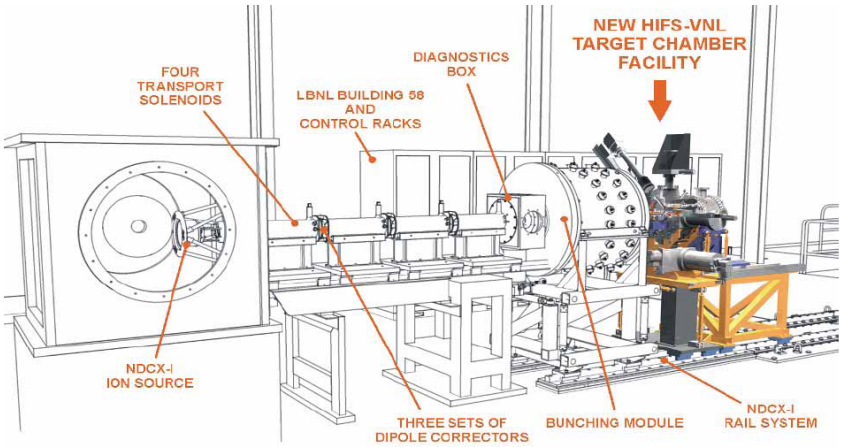

Figure 1: A layout of the NDCX-I accelerator and the WDM target station.

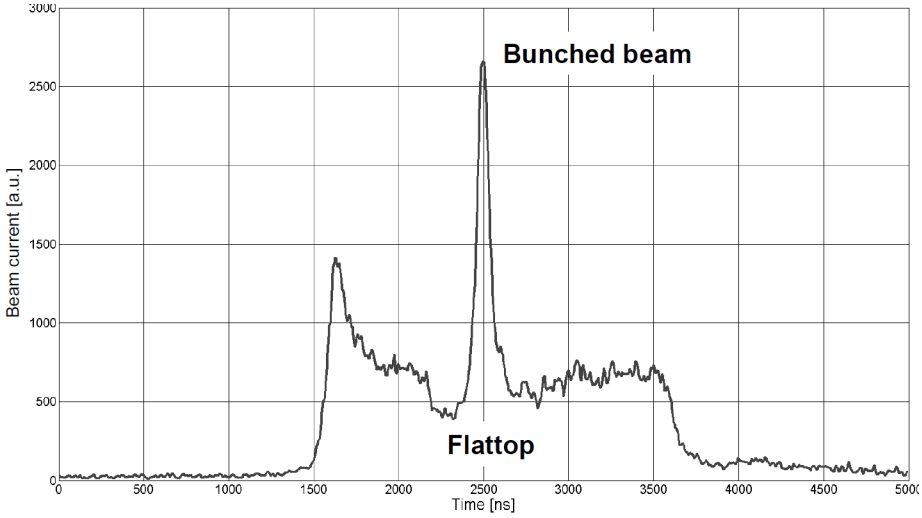

Figure 2: NDCX-I beam pulse structure: a compressed (bunched) pulse sits atop of the uncompressed (flattop) portion of the beam. The pulse can be positioned anywhere within the uncompressed part. It is also possible to have no bunching, with the flattop section only.

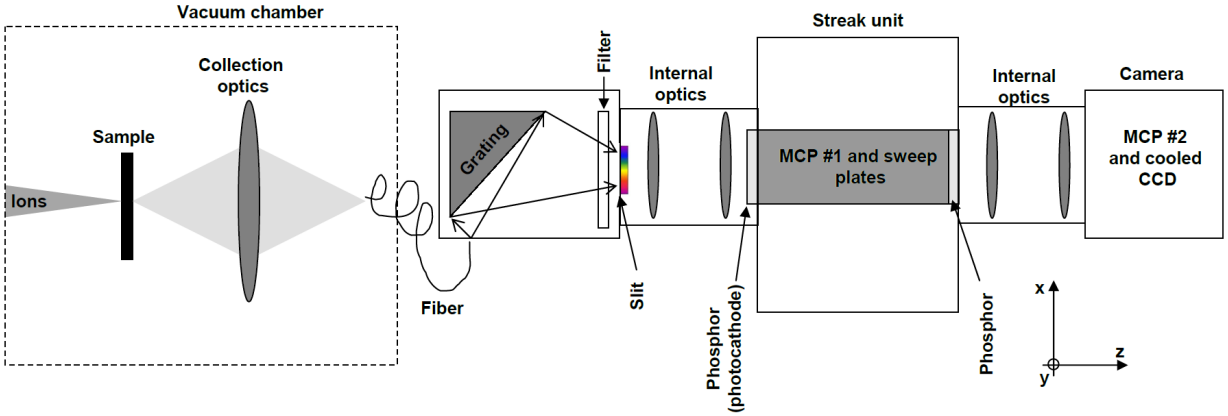

Figure 3: Setup of the experiment.

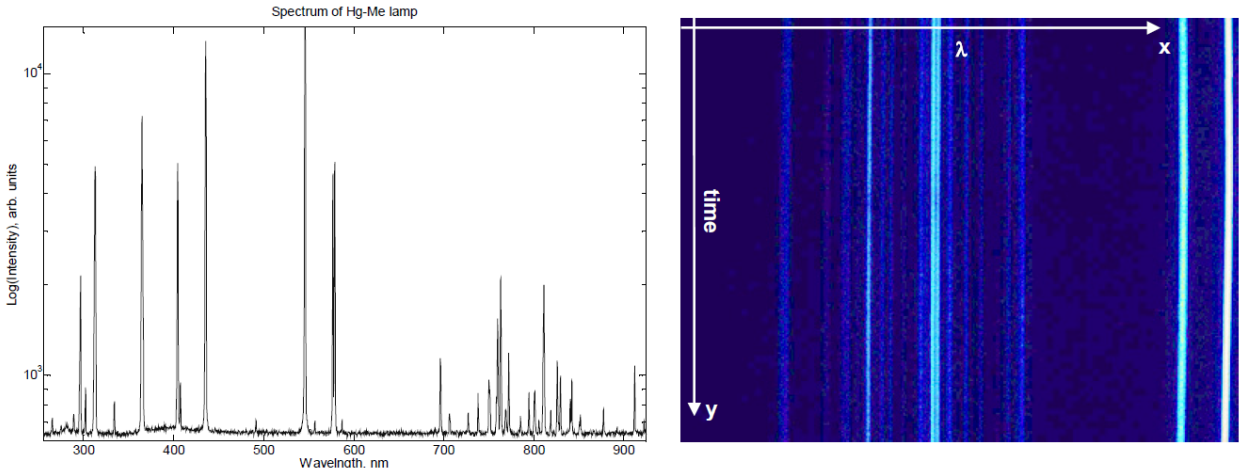

Figure 4: Spectral calibration of the SOP: calibration spectrum of Ar-Hg lamp (left) and corresponding lines recorded by the SOP (right).

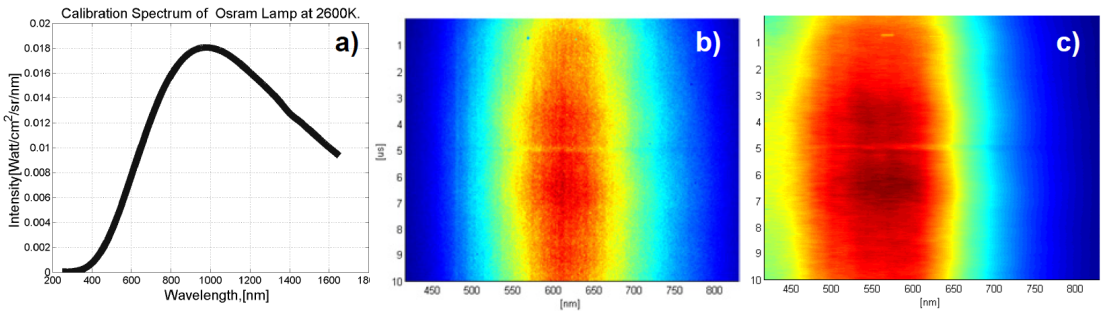

Figure 5: Absolute calibration of the SOP: calibration spectrum of the lamp (a); unprocessed spectral streak image and corresponding calibration image (b). The flat-field correction and defects of the cathode at ~5 µs (position of a slit) are taken into account in the calibration image (c). The calibration conditions: lamp at 2600 K, gain 25, 10 µs sweep Ø200 µm fiber. The streak camera images are shown in false colors.

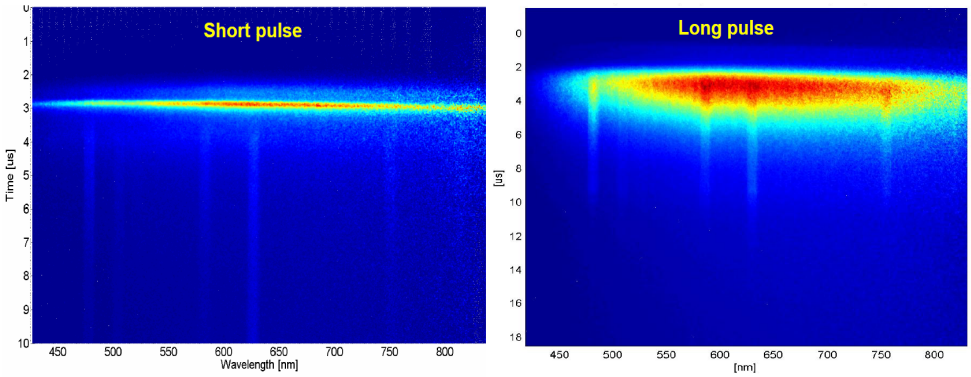

Figure 6: Emission spectra of Au-foils heated with a K^+ ion beam in two experiments with various heating pulses: 2-ns bunched beam (left) and 3-µs uncompressed beam. In the images, beam arrives at the target at 2 µs (left) and at 1 µs (right). Atomic lines correspond to the ion beam-excited Au-I lines (see more details in the text).

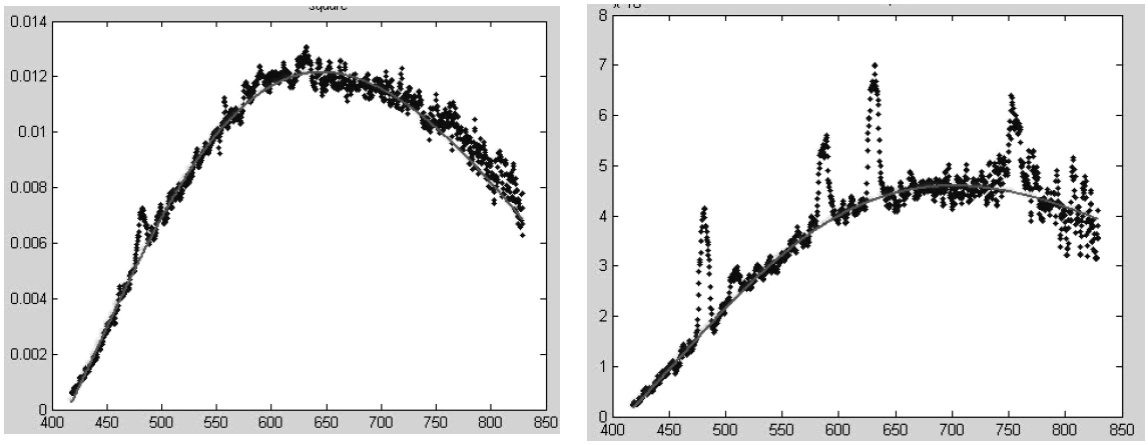

Figure 7: Emission spectra of Au-foils 1.5 μs (Figure 6, left) and 4 μs (s (Figure 6, right)) after arrival of the beam. Gray lines are fitted emission models used for determination of the temperature.

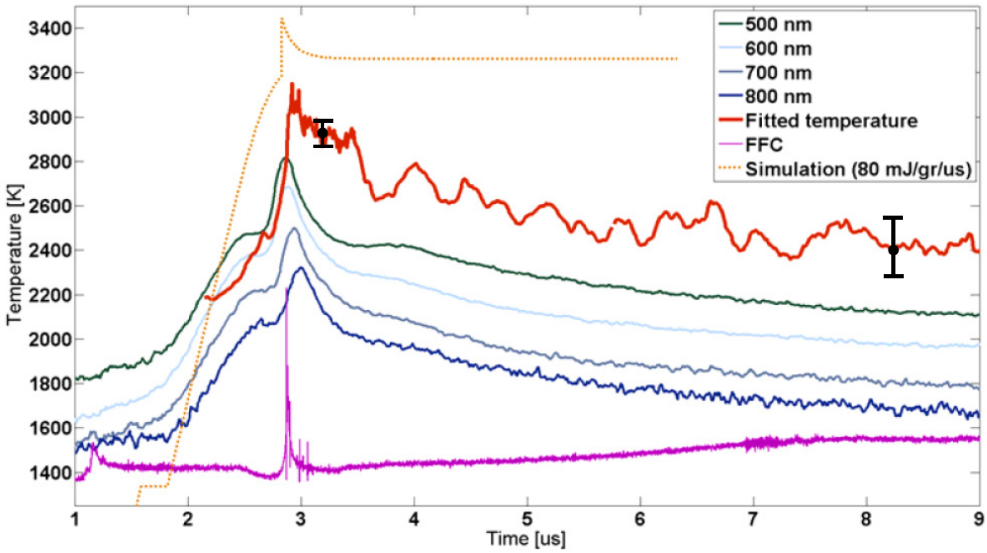

Figure 8: Fitted temperature, black body temperature at various wavelengths, beam current (magenta 'FFC') and corresponding simulation. The results are shown for an experiment in the Figure 6 (left). The error-bar associated with fitting procedure ranges from 5% to 10% (highest value is at the end of record when the signal gets lower).